International Journal of Pharmaceutics 644 (2023) 123341

Contents lists available at ScienceDirect

International Journal of Pharmaceutics

journal homepage: www.elsevier.com/locate/ijpharm

Olfactory drug delivery with intranasal sprays after nasal midvault reconstruction

Harry Chiang [a,*], Hannah L. Martin [a], Ryan M. Sicard [a,b], Dennis O. Frank-Ito [a]

[a] Department of Head and Neck Surgery & Communication Sciences, Duke University, Durham, NC, USA
[b] Icahn School of Medicine at Mount Sinai, New York, NY, USA

ARTICLE INFO

Keywords:
Nose to Brain
Intranasal
Drug Delivery
Olfaction
Midvault Reconstruction
Rhinoplasty

ABSTRACT

Conductive olfaction and nose to brain drug delivery are important processes that remain limited by inadequate odorant or drug delivery to the olfactory airspace. Primary challenges include anatomic barriers and poor targeting to the olfactory region. This study uses computational fluid dynamics to investigate the effects of nasal midvault surgery on olfactory drug delivery with intranasal sprays. Soft tissue elevation, spreader flaps, and spreader grafts were performed on two fresh cadaveric specimens, using computed tomography for airway reconstruction. Nasal airflow and drug particle transport simulations were performed under these conditions: inhalation rate (15, 30 L/min), spray velocity (1, 5, 10 m/s), spray location (top, bottom, center, medial, lateral), head position (upright, supine, forward, backward), and particle size (1–100 μm). Simulation results were used to calculate drug particle deposition to the olfactory airspaces and bulbs. Total olfactory deposition was < 5% but attained a maximum of 36.33% when sorted by particle size. There was no association between nasal midvault surgery and olfactory deposition. No single parameter or technique demonstrated superior olfactory deposition, but smaller particle size, slower spray velocity, and higher inhalation rate tended to optimize olfactory deposition, providing important implications for future intranasal spray and drug design to target the olfactory airspace.

1. Introduction

Conductive olfaction and nose to brain drug delivery are two important processes that share the challenge of drug particle delivery to the olfactory airspace. While olfactory dysfunction has recently been linked to poorer quality of life and increased morbidity (Athanassi et al., 2021; Croy et al., 2014; Gopinath et al., 2012; Kohli et al., 2016; B. Liu et al., 2019), nose to brain (N2B) drug delivery has been shown to provide access to the central nervous system while avoiding systemic toxicity and bypassing the blood brain barrier (Jeong et al., 2023; Keller et al., 2022; Trevino et al., 2020; Z. Wang et al., 2019). Thus, understanding the mechanisms behind these processes has been of growing research interest.

During conductive olfaction (CO), odorant molecules are transported from the nasal vestibule through the complex anatomy of the nasal cavity into the olfactory airspace where they bind to specialized neurons of the olfactory epithelium (Choi & Goldstein, 2018). During N2B drug delivery, a similar process occurs, but upon reaching the olfactory airspace, drug particles have the additional option of traveling along one or more proposed pathways to reach the brain. Direct routes include drug transfer (1) directly along neurons of the olfactory nerve through the cribriform plate, (2) through olfactory epithelial cells at the periphery of the olfactory nerve, and (3) via diffusion, carrier-mediated transport, or other cellular and paracellular mechanisms (Jeong et al., 2023; Trevino et al., 2020). Indirect routes are thought to play a smaller role, as these mechanisms suffer from the same limitations of systemic circulation (Jeong et al., 2023).

Despite multiple potential routes to the brain, N2B drug delivery remains hampered by anatomic challenges and absorptive barriers. Efforts to improve the reliability of N2B delivery have focused on improving delivery devices (e.g., intranasal sprays), drug formulations (e.g., emulsions, mucoadhesive formulations), and drug bioavailability (e.g., permeation enhancers, nanocarriers). Overall, some preliminary studies have been promising, but there is a consensus that inability of sufficient drug particles to reach the olfactory airspace remains a primary challenge (Jeong et al., 2023; Trevino et al., 2020; Yokel, 2022).

* Corresponding author at: Department of Head and Neck Surgery & Communication Sciences, Duke University Medical Center, 40 Duke Medicine Circle, 4028A Yellow Zone, DUMC Box 2824, Durham, NC 27710, USA.
E-mail address: harry.chiang@duke.edu (H. Chiang).

https://doi.org/10.1016/j.ijpharm.2023.123341
Received 19 June 2023; Received in revised form 17 August 2023; Accepted 19 August 2023
Available online 21 August 2023

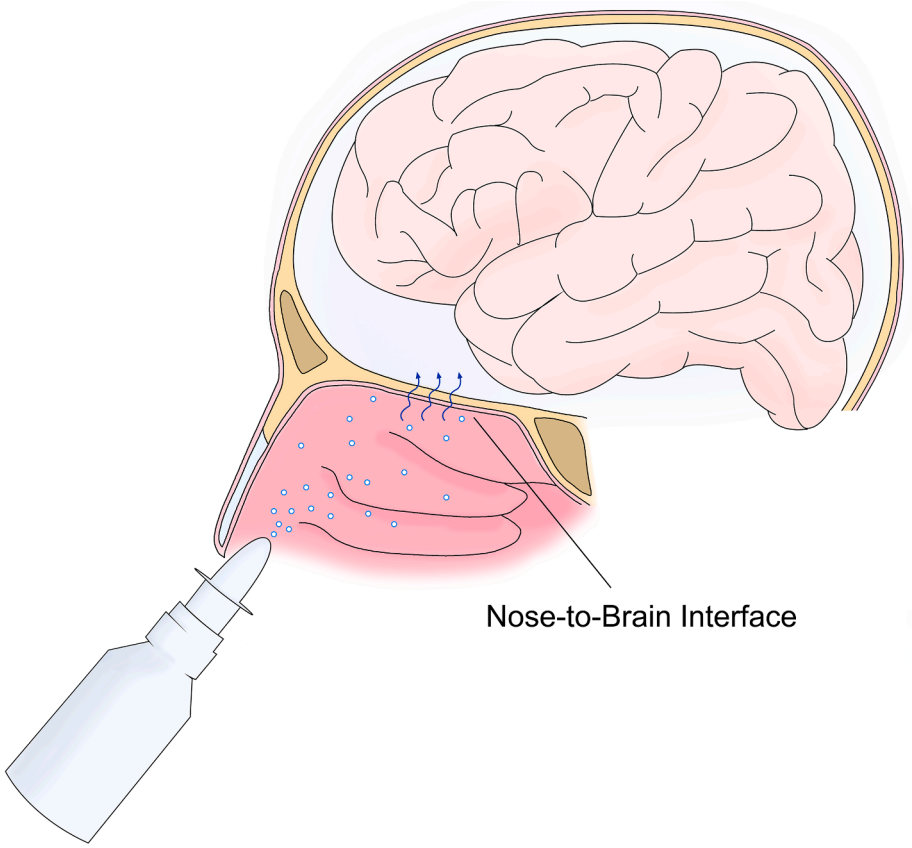

Fig. 1. Schematic of nose-to-brain (N2B) drug delivery using intranasal sprays. Drug particles enter the central nervous system via the nose-to-brain interface.

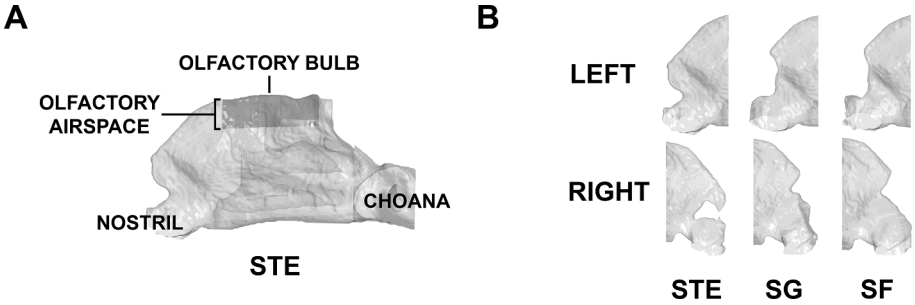

Fig. 2. Example of left nasal cavity model after soft tissue elevation (STE) is shown in A, with anatomic regions of interest labeled: olfactory airspace and olfactory. Effects of nasal midvault reconstruction on left and right anterior nasal anatomy are shown in B, for soft tissue elevation (STE), spreader graft (SG), and spreader flat (SF).

During normal respiration, drug particles are thought to predominantly travel along respiratory airflow streamlines. Previous studies using computational fluid dynamics modeling have found these airflow streamlines and patterns to be heavily dependent on global as well as locoregional nasal anatomy (Brandon et al., 2020; Farzal et al., 2019; Frank-Ito et al., 2019; Lee et al., 2009; Li et al., 2021; Moghaddam et al., 2020), of which the anterior nasal cavity (i.e., nasal vestibule) and nasal midvault are especially important (Garcia et al., 2010; Na et al., 2022; Shadfar et al., 2014; Sicard & Frank-Ito, 2021; T. Wang et al., 2016). However, the effects of nasal anatomy on drug delivery—particularly to the olfactory region—remain poorly characterized. As surgical correction of the anterior nasal cavity and nasal midvault via septoplasty, inferior turbinate reduction, and rhinoplasty are known to improve nasal airflow and relieve nasal obstruction, these anatomic changes are likely to affect drug delivery as well. Intranasal sprays additionally introduce a multitude of factors that can affect drug delivery, including but not limited to nasal spray angle, spray release velocity, and patient position during administration (Basu et al., 2020; Gao et al., 2020; Popper et al., 2022; Schroeter et al., 2006; Xi et al., 2016). An improved understanding of the effects of nasal anatomy and intranasal spray technique on drug delivery to the olfactory airspace (as shown in Fig. 1) could allow for improved intranasal spray device design, refined patient education for optimal spray technique, and individualized assessment of the likelihood of success with topical therapy as well as options for surgical intervention.

This study aims to use computational fluid dynamics to (1) characterize the effects of nasal anatomy on drug particle deposition to the olfactory airspace using two well established midvault nasal reconstruction techniques (spreader grafts and spreader flaps) as a model for controlled variations in nasal anatomy, and (2) identify optimal intranasal spray parameters for targeting drug particles to the olfactory airspace.

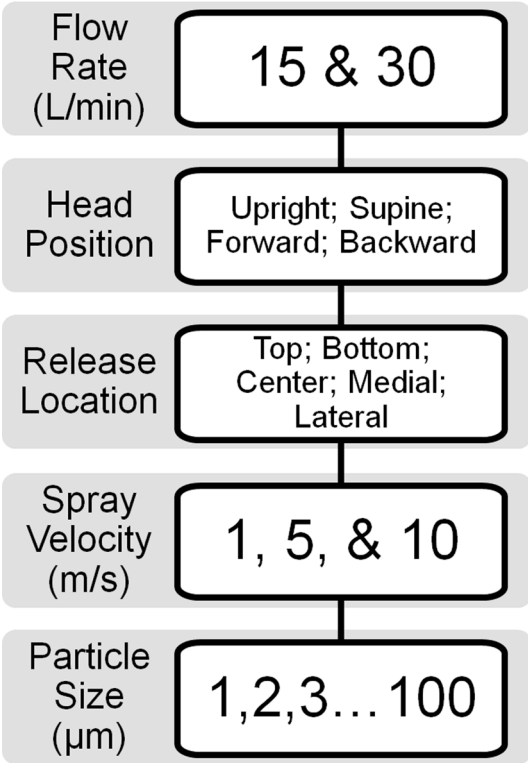

Fig. 3. Schematic of all parameters for particle deposition simulations. All combinations of parameters were tested.

2. Materials and methods

2.1. Nasal midvault reconstruction and imaging

Two fresh frozen cadaveric specimens were included in the study (United Tissue Network, Norman, OK, USA). These specimens had no known history of head or neck cancer, trauma, or prior surgery. Tissue preparation was performed using established methods to remove airway debris and rehydrate the nasal mucosa (Coan et al., 2009). In brief, frozen specimens were defrosted to 65° F and nasal passages were sequentially irrigated with water, rehydrated with isotonic saline, and dried with compressed air (Avashia et al., 2023). For each specimen, a series of three procedures were performed sequentially followed by computed tomography (CT) scan after each procedure. These three procedures were soft tissue elevation (STE) to establish a control for the effects of soft tissue manipulation, spreader grafts (SG), and spreader flaps (SF).

STE was first performed with an open rhinoplasty approach using marginal and transcolumellar incisions. The superficial musculoaponeurotic system (SMAS) was identified, and the soft tissue envelope was elevated to the nasal bones in a sub-SMAS plane. The soft tissue was then re-draped and the skin sutured closed. At this point, CT scan was obtained with the STE stage completed.

SG was then performed using fresh frozen 2 mm cartilage sheet allografts (MTF Biologics, Edison, NJ, USA). These grafts were trimmed to the length of the nasal midvault, as measured from the anterior septal angle to the caudal tip of the nasal bones. The skin was reopened, upper lateral cartilages and dorsal septum were exposed, and the grafts were secured 1 mm below the dorsal septum using two interrupted horizontal mattress 4–0 polydioxanone (PDS) sutures bilaterally. The upper lateral cartilages were then placed over the grafts and sutured to the septum. Soft tissue was re-draped, the skin sutured closed, and CT scan obtained with the SG stage completed.

Lastly, SF was performed. The skin was reopened, the upper lateral cartilages were freed from the septum, and the cartilage grafts were removed. The medial margins of the bilateral upper lateral cartilages were folded inferiorly thus creating spreader flaps and secured using two interrupted horizontal mattress 4–0 PDS sutures. The soft tissue was re-draped, the skin sutured closed, and CT scan once again obtained with the SF stage completed.

2.2. Airspace reconstruction

CT images after each procedure were imported into Avizo Lite™ 9.5.0 (Thermo Fisher Scientific, Waltham, MA, USA) to generate three dimensional reconstructions of the nasal airspaces. Using previously established methods, the nasal airspaces were segmented using the appropriate thresholds with manual tune-up as appropriate (Avashia et al., 2023; Popper et al., 2022; Sicard & Frank-Ito, 2021). Three dimensional models were imported into ICEM-CFD™ 19.0 (ANSYS, Canonsburg, PA, USA) to define anatomic regions of interest in the nasal cavity, and in particular, the olfactory airspace and the olfactory bulb (Fig. 2A). The olfactory airspace was defined as the region from the anterior aspect of the middle turbinate to the anterior face of the sphenoid sinus, from the skull base to 10 mm inferior. The olfactory bulb was defined as the superior surface of the olfactory airspace. Fig. 2B shows the effects of midvault construction on anterior nasal anatomy. At this point, the relevant portions of the nasal airspace were identified,

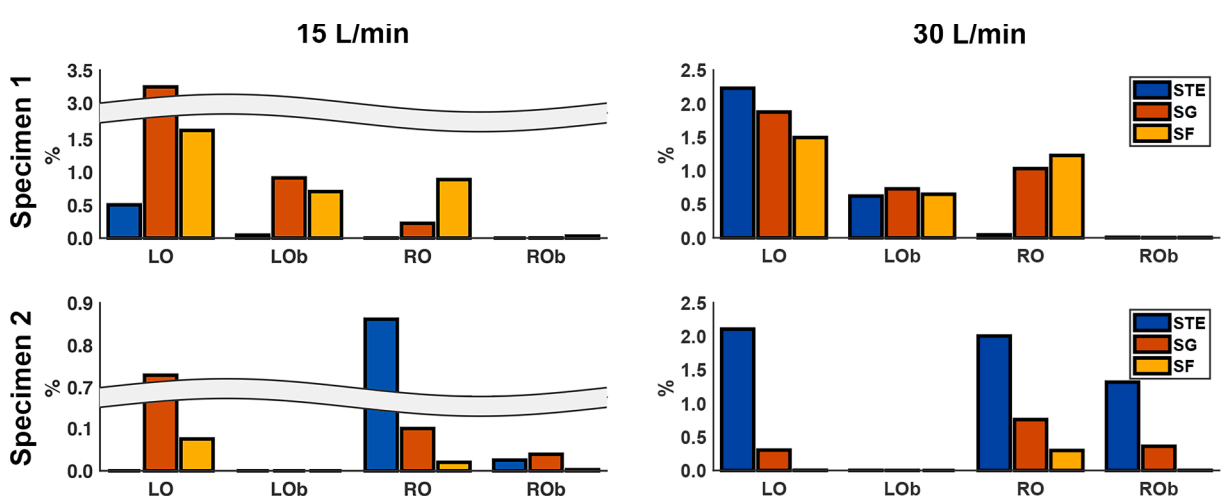

Fig. 4. Maximal total deposition in the olfactory airspaces (O) and olfactory bulbs (Ob) regardless of particle size for specimen 1 (top) and specimen 2 (bottom) for soft tissue elevation (STE), spreader grafts (SG), and spreader flaps (SF), at 15 L/min (left) and 30 L/min (right) inhalation. Gray curve indicates an axis break.

Table 1
Maximal particle deposition in the olfactory airspaces (O) and olfactory bulb (Ob) for each specimen after soft tissue elevation (STE), spreader grafts (SG), and spreader flaps (SF), with corresponding inhalation flow rate, spray release location, head position, particle size, and particle velocity.

	Specimen 1							Specimen 2						
Surgery	Location	Flow Rate (L/m)	Release Location	Head Position	Particle Size (um)	Particle Velocity (m/s)	% Deposition	Location	Flow Rate (L/m)	Release Location	Head Position	Particle Size (um)	Particle Velocity (m/s)	% Deposition
STE	LO	30	Medial	Backward	6–10	1	23.17	LO	30	Top	Supine	6–10	1	36.33
	LOb	30	Medial	Supine	6–10	5	11.78	LOb	30	Top	Supine	6–10	1	0.02
	RO	30	Medial	Upright	1–5	1	0.90	RO	30	Center	Forward	1–5	1	28.35
	ROb	30	Medial	Supine	1–5	1	0.15	ROb	30	Center	Forward	1–5	1	26.34
SG	LO	15	Top	Supine	41–50	1	7.55	LO	15	Lateral	Supine	21–30	1	6.90
	LOb	30	Top	Supine	41–50	1	2.81	LOb	30	Center	Supine	6–10	10	0.01
	RO	30	Top	Backward	6–10	1	17.70	RO	30	Medial	Forward	6–10	1	15.16
	ROb	30	Top	Supine	11–20	1	0.04	ROb	30	Center	Forward	11–20	1	2.65
SF	LO	15	Lateral	Supine	71–80	10	2.78	LO	15	Top	Supine	11–20	5	0.75
	LOb	15	Lateral	Forward	91–100	10	1.45	LOb	—	—	—	—	—	0.00
	RO	30	Top	Backward	6–10	1	11.34	RO	30	Medial	Supine	6–10	5	5.95
	ROb	15	Top	Supine	11–20	1	0.26	ROb	30	Center	Supine	11–20	1	0.10

and the models were ready for airflow and particle delivery simulation.

2.3. Simulation of airflow and olfactory particle delivery

Approximately four million unstructured tetrahedral elements were generated in the nasal airways using ICEM-CFD™ to solve the discretized governing equations of particle fluid dynamics. A four-layer prism-element was created near the walls of the nasal airway. Mesh quality analysis performed to confirm that distorted elements would not impact the accuracy of numerical simulations. Mesh refinement analysis was deferred as the mesh density was chosen based on a detailed mesh sensitivity analysis previously reported (Frank-Ito et al., 2016). With the mesh completed, simulation of particle deposition via intranasal spray was then performed.

Nasal airflow simulation was performed at 15 L/min to simulate resting inspiration and 30 L/min to simulate deep inhalation. For simulation of intranasal spray delivery at 15 L/min, steady laminar incompressible conditions were imposed on the nasal models, and the following boundary conditions were specified: a "mass-flow-outlet" condition at the outlet to target 0.0003 kg/s (15 L/min), atmospheric conditions at the inlet with zero-gauge pressure, and no-slip conditions at the nasal walls as they were considered stationary. For simulation of intranasal spray delivery at 30 L/min, similar boundary conditions were specified, but the "mass-flow-outlet" was specified to target 0.0006 kg/s (30 L/min).

Particle deposition patterns were calculated by simulating the trajectories of spray particles entering the nasal airspace while exchanging mass and momentum with the inspiratory airflow. In Fluent™ 19.0 (ANSYS, Inc., Canonsburg, Pennsylvania, USA), the Euler-Lagrange approach was used for the simulations, assuming unit density of 1000 kg/m^3, spherical particles, and ignoring particle–particle interactions. As outlined in Fig. 3, simulations were performed under all combinations of the following parameters: spray release location (top, bottom, center, medial, lateral), spray velocity (1 m/s, 5 m/s, 10 m/s), head position (upright, supine, forward, backward). Spray release locations were defined as equidistant points along the circumference of a curved surface at a depth of 15 mm (top, bottom, medial, lateral), and the center location as the intersection between lines joining these equidistant points. Monodisperse particles were released at a plume angle of 68° for particle sizes from 1 μm to 100 μm (in 1 μm increments), and 3,500 particles were released into the airway per particle size for a grand total of 350,000 particles. Head positions were defined as upright (in a neutral standing position), supine (lying on the back), forward (tilted forward 45°), and backward (tilted backward 45°). Particles were followed until they either deposited onto a nasal wall or reached the nasopharynx. Each particle was subsequently grouped into the anatomic region of deposition with attention to the olfactory airspace and olfactory bulb. Drug particle deposition percent was calculated as:

$$DF_i = \frac{DP_i}{TP} \times 100\%,$$

where DF_i is deposition fraction in anatomic region i (olfactory airspace or olfactory bulb), DP_i is number of drug particles deposited in anatomic region i, and TP is the total number of drug particles released into the airway.

3. Results

3.1. Total olfactory particle deposition

Maximal total olfactory depositions across all particle sizes are shown for each specimen and procedure in Fig. 4. Deposition percent was calculated targeting (1) the olfactory airspace walls where olfactory epithelium is located, to study olfaction and (2) the olfactory bulb, defined as the superior aspect of the olfactory airspace where direct routes to the brain occur, to study N2B delivery. In general, total particle

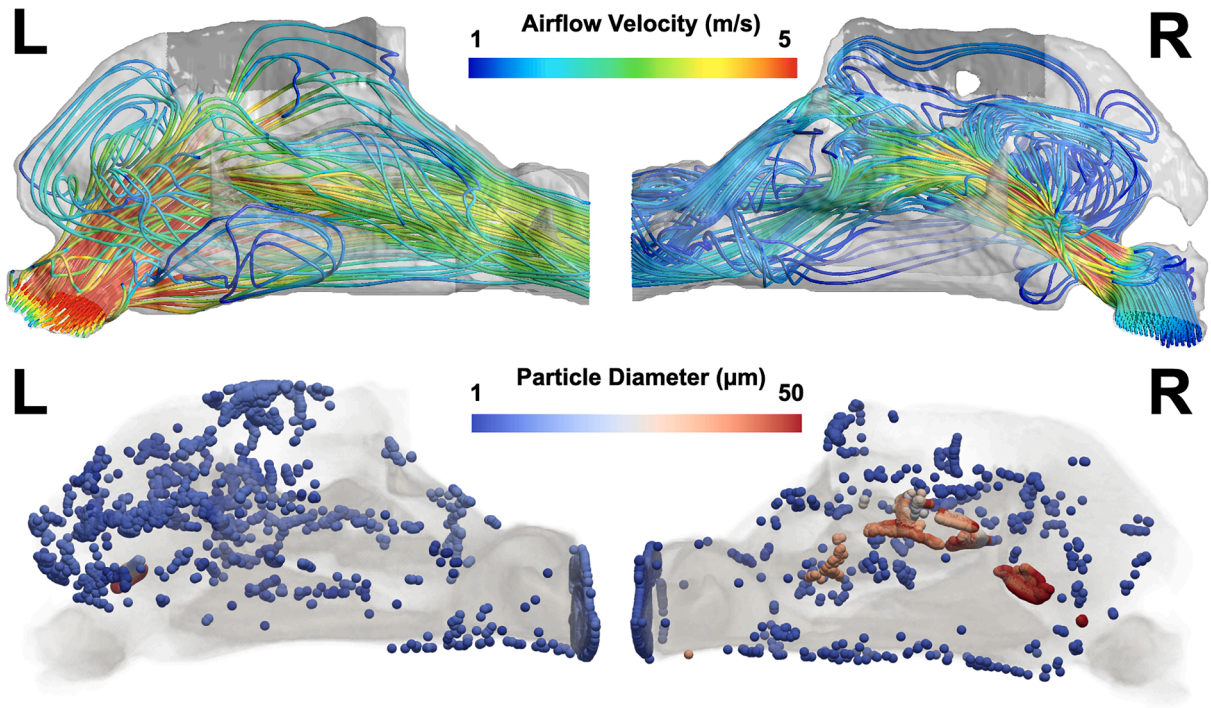

Fig. 5. Airflow streamlines (top) and particle deposition (bottom) for a representative specimen. Note the bilateral notched nasal vestibular phenotypes, where light gray demonstrates nasal airspace with dark gray shadow indicating olfactory airspace.

deposition to each unilateral olfactory airspace and olfactory bulb was low, <5% across both specimens and all procedures. The percentage particle deposition also varied by procedure and all tested parameters: intranasal spray release position, head position, and spray velocity.

For specimen 1 at 15 L/min inspiration to simulate nasal breathing at rest, maximal particle deposition on the left olfactory airspace for each procedure was STE = 0.50%, SG = 3.25%, and SF = 1.63%; for the left olfactory bulb, this was STE = 0.05%, SG = 0.91%, and SF = 0.71%. Maximal particle deposition on the right was generally lower than on the left. Maximal deposition on the right olfactory airspace was STE = 0.00%, SG = 0.22%, and SF = 0.89%; for the right olfactory bulb, this was STE = 0.00%, SG = 0.00%, SF = 0.03%. At 30 L/min inspiration to simulate deep inspiration or sniffing, maximal particle deposition on the left olfactory airspace for each procedure was STE = 2.23%, SG = 1.87%, and SF = 1.50%; for the left olfactory bulb, this was STE = 0.62%, SG = 0.73%, and SF = 0.65%. Maximal deposition on the right was again generally lower than on the left. Maximal deposition on the right olfactory airspace was STE = 0.04%, SG = 1.03%, and SF = 1.23%; for the right olfactory bulb, this was STE = 0.01%, SG = 0.00%, and SF = 0.01%.

For specimen 2 at 15 L/min inspiration, maximal particle deposition on the left olfactory airspace for each procedure was STE = 0.00%, SG = 0.73%, and SF = 0.07%; there was no deposition on the left olfactory bulb for all procedures. Maximal particle deposition on the right was comparable to that on the left. Maximal deposition on the right olfactory airspace was STE = 0.86%, SG = 0.10, and SF = 0.02%; for the right olfactory bulb, this was STE = 0.03%, SG = 0.04%, and SF = 0.00%. At 30 L/min inspiration, maximal particle deposition on the left olfactory airspace for each procedure was STE = 2.10%, SG = 0.30%, and SF = 0.00%; there was no deposition on the left olfactory bulb for all procedures. Maximal deposition on the right olfactory airspace was STE = 2.00%, SG = 0.76, and SF = 0.30%; for the right olfactory bulb, this was STE = 1.32, SG = 0.36, and SF = 0.00%.

3.2. Particle size distribution

Deposition in the olfactory airspace and olfactory bulb across the following particle size bins was determined: 1–5 μm, 6–10 μm, and then in groups of 10 μm for the remainder of particle size ranges (i.e., 11–20 μm, 21–30 μm, …, 91–100 μm). For specimen 2, optimal delivery to the olfactory airspace and olfactory bulb tended to occur for smaller particles (≤20 μm) in 10 out of 11 cases, but this pattern was not as clearly seen for specimen 1 (8 out of 12 cases with ≤ 20 μm), as shown in Table 1. No particles reached the left olfactory bulb in specimen 2 for all procedures, and no particles reached either left or right olfactory bulbs in specimen 2 SF. Representative distribution of particle deposition with airflow streamlines in the nasal cavity by size is shown in Fig. 5.

3.3. Optimal parameters for olfactory particle delivery

When identifying optimal delivery parameters while factoring in particle size, percentage deposition to the olfactory airspace and olfactory bulb varied more widely across specimens, ranging 0.00–36.33%. The optimal parameter combinations leading to maximal deposition are shown in Table 1. Overall, there was no single surgical procedure, inspiratory rate, release location, head position, particle velocity, or particle size, that was consistently associated with increased particle delivery to the olfactory airspace for either specimen, although smaller particles tended to reach the olfactory regions more readily than larger particles, as described in Section 3.2. With narrow particle size bins of range 10 μm or less, the deposition efficiency was notably increased, compared to with wide particle size bins of 1–100 μm (Fig. 6). This effect was observed both in drug delivery to the olfactory airspaces and to the olfactory bulbs across all experiments except those with no olfactory deposition. In many cases, the deposition efficiency was increased by 1 or more order of magnitude.

There also appeared to be a predilection for slower particle velocity of 1 m/s (17 out of 23 cases) and for higher inspiratory rate of 30 L/min (17 out of 23 cases). Optimal spray release location and head position varied widely across specimens and procedures. Notably, in several

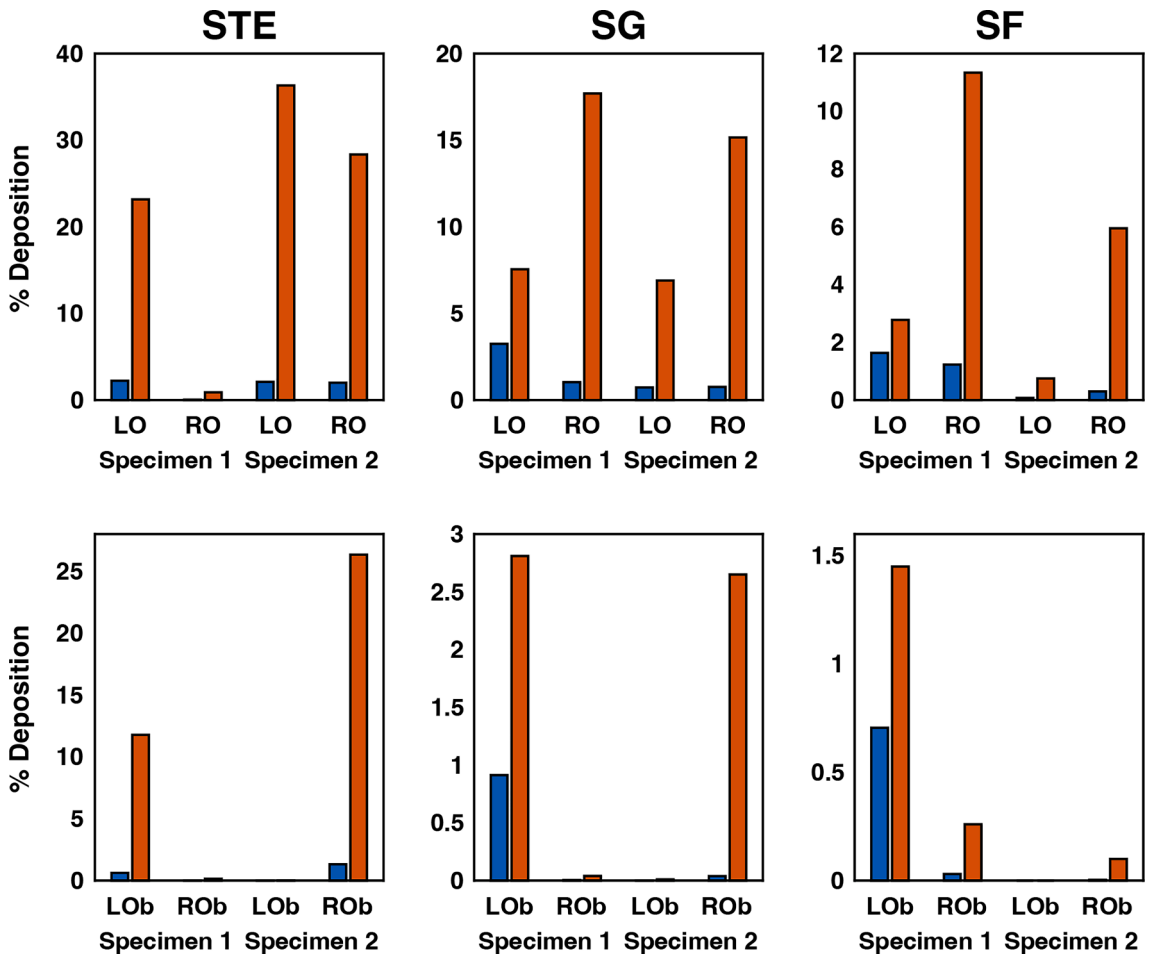

Fig. 6. Optimal deposition efficiency to the olfactory airspaces (O) and olfactory bulbs (Ob) with wide particle size range of 1–100 μm (blue), and narrow particle size bins of 10 μm or less (red) for each specimen after soft tissue elevation (STE), spreader grafts (SG), and spreader flaps (SF).

cases, the optimal inspiratory flow rate, release location, head position, particle size, and particle velocity were different for delivery to the olfactory airspace versus the olfactory bulb despite the same anatomy (same specimen and procedure group).

4. Discussion

The relatively low rates of olfactory particle deposition < 5% in this study are consistent with the challenging nature of drug delivery to the olfactory region (Garcia et al., 2015; Schroeter et al., 2006; Xi et al., 2016). Previous studies using CFD simulation and experimental models have estimated olfactory particle deposition during inhalation to be < 1–4% (Si & Xi, 2016; Vachhani & Kleinstreuer, 2021), but with the use of intranasal sprays, deposition efficiency can be greatly enhanced, albeit with more variable results (Kiaee et al., 2018). Olfactory deposition efficiency has been shown to range widely across patients, up to 2 orders of magnitude (Kiaee et al., 2018). These discrepancies are largely attributed to the highly sensitive interactions between nasal anatomy and olfactory delivery. In the present study, particle deposition using intranasal sprays (when arranged by particle size) attained a maximum of 36.33% to the unilateral olfactory region at 6–10 μm, and 26.34% to the olfactory bulb at 1–5 μm. However, the optimal spray parameters to achieve these deposition rates for each specimen and each procedure group varied widely and were thus dependent on the individual nasal anatomy. Moreover, the optimal spray parameters to achieve maximal deposition to the olfactory regions were also in several cases different from the optimal parameters to achieve maximal deposition to the olfactory bulb. Thus, even the nuanced anatomical differences within the olfactory region are likely to play a role in N2B delivery, further highlighting the sensitive interactions between nasal anatomy and olfactory delivery. In summary, there was no single set of intranasal spray administration parameters that consistently improved particle delivery to either the olfactory region or the olfactory bulb.

Nonetheless, some trends were found to be associated with increased olfactory delivery. Smaller particles (≤20 μm) tended to have a higher likelihood of reaching the olfactory space, while larger particles (greater than50 μm) tended to be captured by the anterior nasal cavity. This trend has been seen in other studies as well (Kiaee et al., 2018; Kimbell et al., 2007; Vachhani & Kleinstreuer, 2021). Moreover, narrow particle size ranges (with smaller particles) were associated with dramatically increased deposition efficiency over wide particle size ranges, often by more than an order of magnitude. The significance of this finding is that current commercially available sprays tend to produce a wide range of particle sizes, and that the mean droplet size is typically on the order of 50–70 μm in diameter (Si & Xi, 2016). Moreover, particles ≤ 10 μm are thought to risk entry into the lower airway, potentially causing harm to the lungs. Thus, current spray devices at the outset are at a disadvantage for olfactory delivery due to (1) large particle trapping in the anterior nasal cavity and (2) limited particle size ranges that can efficiently reach the olfactory epithelium while avoiding pulmonary toxicity (Ehrick et al., 2013; Gisle Djupesland et al., 2004; Kiaee et al., 2018). Slower spray velocity also tended to increase olfactory delivery. Intranasal spray velocity from commercially available products has been previously researched using a variety of methods and have been found to range from ~ 5–20 m/s (X. Liu et al., 2011). These velocities are greater than 1 m/s, which in general, delivered particles to the olfactory region

most effectively in this study. Droplet size and spray velocity are both parameters that are dependent on actuation pressure from hand-generated aerosols (Inthavong et al., 2015) and should be considered in future device design.

Although the current models do not capture the effects of nasal midvault reconstruction on dynamic nasal valve collapse, spreader grafts and spreader flaps do not appear to strongly influence particle delivery to the olfactory region. It is also important to note that the cadaveric population selected for this study are not the typical patients with internal nasal valve dysfunction undergoing these procedures; thus, the benefits of the spreader grafts and spreader flaps may not be fully captured by the associated change in anatomy for the basis of the model. However, recent comparisons between CT images of preoperative and postoperative rhinoplasty subjects have similarly been unable to identify differences in internal nasal valve angle and internal nasal valve area despite improved postoperative NOSE scores (Shafik et al., 2020). This suggests that the primary means of improving internal nasal valve function with rhinoplasty and midvault reconstruction may be the increased support to the soft tissue, rather than the widening of the valve angle. Therefore, the primary utility of this model is studying controlled variations in nasal anatomy of cadaveric specimens rather than representing the dynamic effects of surgery in vivo. Further exploration of different nasal procedures including virtual surgeries will improve understanding of the effects of anatomic variations on olfactory deposition. Indeed, virtual surgeries are a primary advantage of CFD analysis due to the ability to digitally simulate postoperative nasal anatomy, whereas experimental models of aerosol delivery provide a means for validating computational results. During intranasal spray in vivo, there is also the additional effect of stenting at the external nasal valve with the spray tip. Though this model does not account for nasal valve stenting, it simulates an insertion depth of 15 mm to bypass the anterior-most aspect of the nasal vestibule. For future work, the effects of increased nasal valve rigidity during spray delivery would better be characterized with a dynamic model, and surgical procedures that produce other static anatomic changes should be investigated as well. In addition, CFD can be used to investigate the impact of spray pattern or plume geometry, which is likely to affect olfactory deposition patterns (Ehrick et al., 2013).

5. Conclusions

This study used computational fluid dynamics to investigate the impact of nasal midvault reconstruction on olfactory drug delivery using intranasal sprays. There was no change in olfactory deposition from the static effects of spreader grafts and spreader flaps. There was also no single intranasal spray parameter or technique that was consistently associated with increased olfactory deposition, but smaller particle size, slower spray velocity, and higher inhalation rate during administration tended to optimize olfactory deposition.

CRediT authorship contribution statement

Harry Chiang: Conceptualization, Methodology, Software, Investigation. **Hannah L. Martin:** Data curation, Software. **Ryan M. Sicard:** Data curation, Software, Visualization. **Dennis O. Frank-Ito:** Conceptualization, Supervision.

Declaration of Competing Interest

The authors declare that they have no known competing financial interests or personal relationships that could have appeared to influence the work reported in this paper.

Data availability

The data that has been used is confidential.

Acknowledgements

This research was supported by the Aesthetic Surgery Education and Research Foundation (ASERF). Funds were used for procurement of cadaveric specimens, computer software for computational analysis, computed-tomography scanning, and other direct study costs. The content of this manuscript is the responsibility of the authors and does not necessarily represent the views of ASERF. In addition, special thanks to ANSYS, ANSYS Global Academic Program, and Dr. Paolo Maccarini (Duke University) for support and strategic donation. All authors gave final approval for publication.

References

Athanassi, A., Dorado Doncel, R., Bath, K.G., Mandairon, N., 2021. Relationship between depression and olfactory sensory function: A review. In: Chemical Senses, Vol. 46. Oxford University Press. https://doi.org/10.1093/chemse/bjab044.

Avashia, Y.J., Martin, H.L., Frank-Ito, D.O., Hodges, K.Z., Trotta, R.T., Li, H., Lowry, C., Woodard, C.R., Allori, A.C., Marcus, J.R., 2023. Computational Analyses of Physiologic Effects After Midvault Repair Techniques in Rhinoplasty. FACE 4 (1), 22–32. https://doi.org/10.1177/27325016221138749.

Basu, S., Holbrook, L.T., Kudlaty, K., Fasanmade, O., Wu, J., Burke, A., Langworthy, B. W., Farzal, Z., Mamdani, M., Bennett, W.D., Fine, J.P., Senior, B.A., Zanation, A.M., Ebert, C.S., Kimple, A.J., Thorp, B.D., Frank-Ito, D.O., Garcia, G.J.M., Kimbell, J.S., 2020. Numerical evaluation of spray position for improved nasal drug delivery. Sci. Rep. 10 (1) https://doi.org/10.1038/s41598-020-66716-0.

Brandon, B.M., Stepp, W.H., Basu, S., Kimbell, J.S., Senior, B.A., Shockley, W.W., Madison Clark, J., 2020. Nasal Airflow Changes With Bioabsorbable Implant, Butterfly, and Spreader Grafts. Laryngoscope 130 (12), E817–E823. https://doi.org/10.1002/lary.28691.

Choi, R., Goldstein, B.J., 2018. Olfactory epithelium: Cells, clinical disorders, and insights from an adult stem cell niche. In: Laryngoscope Investigative Otolaryngology, Vol. 3(1). John Wiley and Sons Inc., pp. 35–42. https://doi.org/10.1002/lio2.135

Coan, B.S., Neff, E., Mukundan, S., Marcus, J.R., 2009. Validation of a cadaveric model for comprehensive physiologic and anatomic evaluation of rhinoplastic techniques. Plast. Reconstr. Surg. 124 (6), 2107–2117. https://doi.org/10.1097/PRS.0b013e3181bf7e3a.

Croy, I., Nordin, S., Hummel, T., 2014. Olfactory disorders and quality of life-an updated review. Chem. Senses 39 (3), 185–194. https://doi.org/10.1093/chemse/bjt072.

Djupesland, P.G., Skretting, A., Winderen, M., Holand, T., 2004. Bi-Directional Nasal Delivery of Aerosols Can Prevent Lung Deposition. J. Aerosol Med. 17 (3), 249–259.

Ehrick, J. D., Shah, S. A., Shaw, C., Kulkarni, V. S., Coowanitwong, I., De, S., & Suman, J. D. (2013). *Considerations for the Development of Nasal Dosage Forms* (pp. 99–144). https://doi.org/10.1007/978-1-4614-7978-9_5.

Farzal, Z., Signore, A.G.D., Zanation, A.M., Ebert, C.S., Frank-Ito, D., Kimbell, J.S., Senior, B.A., 2019. A computational fluid dynamics analysis of the effects of size and shape of anterior nasal septal perforations. Rhinology 57 (2), 153–159. https://doi.org/10.4193/Rhin18.111.

Frank-Ito, D.O., Wofford, M., Schroeter, J.D., Kimbell, J.S., 2016. Influence of Mesh Density on Airflow and Particle Deposition in Sinonasal Airway Modeling. J. Aerosol Med. Pulm. Drug Deliv. 29 (1), 46–56. https://doi.org/10.1089/jamp.2014.1188.

Frank-Ito, D.O., Carpenter, D.J., Cheng, T., Avashia, Y.J., Brown, D.A., Glener, A., Allori, A., Marcus, J.R., 2019. Computational Analysis of the Mature Unilateral Cleft Lip Nasal Deformity on Nasal Patency. Plastic and Reconstructive Surgery - Global Open 7 (5), E2244. https://doi.org/10.1097/GOX.0000000000002244.

Gao, M., Shen, X., Mao, S., 2020. Factors influencing drug deposition in the nasal cavity upon delivery via nasal sprays. J. Pharm. Investig. 50 (3), 251–259. https://doi.org/10.1007/s40005-020-00482-z. Springer.

Garcia, G.J.M., Rhee, J.S., Senior, B.A., Kimbell, J.S., 2010. Septal deviation and nasal resistance: An investigation using virtual surgery and computational fluid dynamics. Am. J. Rhinol. Allergy 24 (1), e46–e53. https://doi.org/10.2500/ajra.2010.24.3428.

Garcia, G.J.M., Schroeter, J.D., Kimbell, J.S., 2015. Olfactory deposition of inhaled nanoparticles in humans. Inhal. Toxicol. 27 (8), 394–403. https://doi.org/10.3109/08958378.2015.1066904.

Gopinath, B., Sue, C.M., Kifley, A., Mitchell, P., 2012. The association between olfactory impairment and total mortality in older adults. J. Gerontol. Ser. A Biol. Sci. a Med. Sci. 67 (A(2)), 204–209. https://doi.org/10.1093/gerona/glr165.

Inthavong, K., Fung, M.C., Yang, W., Tu, J., 2015. Measurements of droplet size distribution and analysis of nasal spray atomization from different actuation pressure. J. Aerosol Med. Pulm. Drug Deliv. 28 (1), 59–67. https://doi.org/10.1089/jamp.2013.1093.

Jeong, S.-H., Jang, J.-H., Lee, Y.-B., 2023. Drug delivery to the brain via the nasal route of administration: exploration of key targets and major consideration factors. J. Pharm. Investig. 53 (1), 119–152. https://doi.org/10.1007/s40005-022-00589-5.

Keller, L.A., Merkel, O., Popp, A., 2022. Intranasal drug delivery: opportunities and toxicologic challenges during drug development. Drug Deliv. Transl. Res. 12 (4), 735–757. https://doi.org/10.1007/s13346-020-00891-5.

Kiaee, M., Wachtel, H., Noga, M.L., Martin, A.R., Finlay, W.H., 2018. Regional deposition of nasal sprays in adults: A wide ranging computational study. Int. J. Numer. Methods Biomed. Eng. 34 (5), e2968.

Kimbell, J.S., Segal, R.A., Asgharian, B., Wong, B.A., Schroeter, J.D., Southall, J.P., Dickens, C.J., Brace, G., Miller, F.J., 2007. Characterization of deposition from nasal spray devices using a computational fluid dynamics model of the human nasal passages. J. Aerosol Med. Depos. Clear. Effects the Lung 20 (1), 59–74. https://doi.org/10.1089/jam.2006.0531.

Kohli, P., Soler, Z.M., Nguyen, S.A., Muus, J.S., Schlosser, R.J., 2016. The association between olfaction and depression: A systematic review. In: Chemical Senses, Vol. 41 (6). Oxford University Press, pp. 479–486. https://doi.org/10.1093/chemse/bjw061.

Lee, H.P., Poh, H.J., Chong, F.H., Wang, D.Y., 2009. Changes of airflow pattern in inferior turbinate hypertrophy: A computational fluid dynamics model. Am. J. Rhinol. Allergy 23 (2), 153–158. https://doi.org/10.2500/ajra.2009.23.3287.

Li, L., Zang, H., Han, D., London, N.R., 2021. Impact of Varying Types of Nasal Septal Deviation on Nasal Airflow Pattern and Warming Function: A Computational Fluid Dynamics Analysis. Ear Nose Throat J. 100 (6), NP283–N2P9.

Liu, X., Doub, W.H., Guo, C., 2011. Assessment of the influence factors on nasal spray droplet velocity using Phase-Doppler Anemometry (PDA). AAPS PharmSciTech 12 (1), 337–343. https://doi.org/10.1208/s12249-011-9594-1.

Liu, B., Luo, Z., Pinto, J.M., Shiroma, E.J., Tranah, G.J., Wirdefeldt, K., Fang, F., Harris, T.B., Chen, H., 2019. Relationship between poor olfaction and mortality among community-dwelling older adults: A cohort study. Ann. Intern. Med. 170 (10), 673–681. https://doi.org/10.7326/M18-0775.

Moghaddam, M.G., Garcia, G.J.M., Frank-Ito, D.O., Kimbell, J.S., Rhee, J.S., 2020. Virtual septoplasty: a method to predict surgical outcomes for patients with nasal airway obstruction. Int. J. Comput. Assist. Radiol. Surg. 15 (4), 725–735. https://doi.org/10.1007/s11548-020-02124-z.

Na, Y., Kwon, K.W., Jang, Y.J., 2022. Impact of the Location of Nasal Septal Deviation on the Nasal Airflow and Air Conditioning Characteristics. Facial Plast. Surg. https://doi.org/10.1055/s-0042-1759764.

Popper, C., Martin, H., Shah, R., Sicard, R., Hodges, K., Frank-Ito, D.O., 2022. Intranasal Spray Characteristics for Best Drug Delivery in Patients With Chronic Rhinosinusitis. Laryngoscope. https://doi.org/10.1002/lary.30155.

Schroeter, J.D., Kimbell, J.S., Asgharian, B., 2006. Analysis of Particle Deposition in the Turbinate and Olfactory Regions Using a Human Nasal Computational Fluid Dynamics Model. J. Aerosol Med. 19 (3), 301–313.

Shadfar, S., Shockley, W.W., Fleischman, G.M., Dugar, A.R., McKinney, K.A., Frank-Ito, D.O., Kimbell, J.S., 2014. Characterization of postoperative changes in nasal airflow using a cadaveric computational fluid dynamics model: Supporting the internal nasal valve. JAMA Facial Plastic Surgery 16 (5), 319–327. https://doi.org/10.1001/jamafacial.2014.395.

Shafik, A.G., Alkady, H.A., Tawfik, G.M., Mohamed, A.M., Rabie, T.M., Huy, N.T., 2020. Computed tomography evaluation of internal nasal valve angle and area and its correlation with NOSE scale for symptomatic improvement in rhinoplasty. Braz. J. Otorhinolaryngol. 86 (3), 343–350. https://doi.org/10.1016/j.bjorl.2019.08.009.

Si, X.A., Xi, J., 2016. Modeling and simulations of olfactory drug delivery with passive and active controls of nasally inhaled pharmaceutical aerosols. J. Vis. Exp. 2016 (111) https://doi.org/10.3791/53902.

Sicard, R.M., Frank-Ito, D.O., 2021. Role of nasal vestibule morphological variations on olfactory airflow dynamics. Clin. Biomech. 82, 105282.

Trevino, J. T., Quispe, R. C., Khan, F., & Novak, V. (2020). *Non-Invasive Strategies for Nose-to-Brain Drug Delivery*.

Vachhani, S., Kleinstreuer, C., 2021. Comparison of micron- and nano-particle transport in the human nasal cavity with a focus on the olfactory region. Comput. Biol. Med. 128, 104103.

Wang, T., Chen, D., Wang, P.H., Chen, J., Deng, J., 2016. Investigation on the nasal airflow characteristics of anterior nasal cavity stenosis. Brazilian C Biol. Res. 49 (9) https://doi.org/10.1590/1414-431X20165182.

Wang, Z., Xiong, G., Tsang, W.C., Schätzlein, A.G., Uchegbu, I.F., 2019. Nose-to-brain delivery. J. Pharmacol. Exp. Ther. 370 (3), 593–601. https://doi.org/10.1124/jpet.119.258152. American Society for Pharmacology and Experimental Therapy.

Xi, J., Yuan, J.E., Zhang, Y., Nevorski, D., Wang, Z., Zhou, Y., 2016. Visualization and Quantification of Nasal and Olfactory Deposition in a Sectional Adult Nasal Airway Cast. Pharm. Res. 33 (6), 1527–1541. https://doi.org/10.1007/s11095-016-1896-2.

Yokel, R.A., 2022. Direct nose to the brain nanomedicine delivery presents a formidable challenge. In: Wiley Interdisciplinary Reviews: Nanomedicine and Nanobiotechnology, Vol. 14, Issue 2. John Wiley and Sons Inc. https://doi.org/10.1002/wnan.1767